Contents lists available at Science-Gate

International Journal of Advanced and Applied Sciences

Journal homepage: http://www.science-gate.com/IJAAS.html

Nuclear research reactor simulator

Ramin Barati *

Department of Electrical Engineering, Shiraz Branch, Islamic Azad University, Shiraz, Iran

ARTICLE INFO

Article history:
Received 27 March 2015
Received in revised form
5 May 2015
Accepted 7 May 2015

Keywords:
Dynamics modelling
Fuel burn up
Point kinetics model
Research reactors

ABSTRACT

In this paper, a useful simulator is presented to simulate the kinetics and dynamics of a research reactor core. The model considers relevant physical phenomena that govern the core such as reactor kinetics, reactivity feedbacks due to coolant and fuel temperatures (Doppler effects) with variable reactivity coefficients, xenon, samarium, boron concentration, fuel burn up and thermal hydraulics. WIMS and CITVAP codes are used to extract neutron cross sections and calculate the initial neuron flux respectively. The purpose is to present a model with results similar to reality as much as possible with reducing common simplifications in reactor modeling to be used in different analyses such as reactor control, functional reliability, safety and etc.

1. Introduction

In order to analyze complex phenomena such as nuclear research reactors to be used in control, safety, and functional reliability issues, it is necessary to include different parameters of reactor as much as possible to reduce errors related to common simplifications such as works done by (Arab-Alibeik and Setayeshi, 2003, 2005; Ben-Abdennour et al., 1992; Edwards et al., 1992; Arab-Alibeik and Setayeshi, 2003) which underestimate the complexity of phenomena.

Many codes have been developed for the analysis of some anticipated transients and accidents concerned about nuclear reactors, such as RELAP, RETRAN, CATHARE, and ATHLET (Qing Lu et al., 2009). However, most of these tools were developed for power reactors and their application to research reactors is not straightforward and in sometimes even improper (Hamidouche et al., 2004) and (Woodruff, 1996). Also, even for power reactor they use simplified neutronic calculations which are not the true representation for the reactor complexity. In general, an issue in this problem could be the use of power reactor's code including some procedures and models suitable for the operating conditions of research reactors. In order to apply this type of codes in the analysis of a research reactor, (Hainoun, 2003) has modified or added some procedures and models which are suitable for the operating condition of a research reactor. Furthermore, much work has been done to investigate the research reactor by developing a code with relatively simple but proper physical models (Bousbia Salah and Hamidouche, 2005), (El-Messiry, 2000), (Mariy et al., 2003), (Kazeminejad, 2008), (Hany et al., 2007), (Nabbi, 1995), and (Woodruff, 1984). However, these works, because of their simplifications in neutronic calculations and using constant fuel and coolant temperature reactivity coefficients are not the true representation of complexity of reactor core.

In this study, a thirty fourth order model is presented which in contrast with the previous works, considers delayed neutrons fraction as a function of time and variable fuel and temperature reactivity coefficients which can be used for the core evaluation in transient states. Real time simulating while taking less simplification into account make this model effective in safety, control, and functional reliability issues both in research and power reactors.

In the 34th order dynamics model presented in this article, the equations for neutron kinetics, thermal hydraulics and changes in nuclide composition during fuel burn-up are solved simultaneously, and they have very different time constants. Therefore, we get a very stiff system of equations. But In order to model a full fuel cycle in a nuclear reactor, it is necessary to simulate the short timescale kinetic behavior of the reactor as well as the long time-scale dynamics that occur with fuel burn up. The former is modeled using the point kinetics equations, while the latter is modeled by coupling fuel burn up equations with the kinetics equations. When the equations are solved simultaneously with a nonlinear equation solver, the end result is a code with the unique capability of modeling transients at any time during a fuel cycle. Indeed, the traditional use of the point reactor kinetics equations is to model transients over short time periods (seconds to minutes). When the

* Corresponding Author.
Email Address: barati@iaushiraz.ac.ir

equations are used for this purpose, time dependence in all kinetics parameters other than the reactivity can be safely neglected without introducing significant error into the model. For short time scales where fuel composition changes are negligible, large changes in the delayed neutron fraction, β, or the mean neutron generation time, Λ, could not occur without a significant departure from criticality that would invalidate the use of the point kinetics model. For longer time scales, the composition changes that affect the point kinetics equations of the fuel cycle for burnup and transmutation are the subject of this research.

For extracting neutron cross sections and initial neutron flux, cell and core calculations are needed (Sadighi et al., 2002). WIMS, BORGES (Rubio, 1993) and CITVAP (new version of the CITATION-II) codes (Villarino and Carlos, 1993) as the well-known computer codes used in MTR_PC code, are used for these calculations. Microscopic cross section sets generated by WIMS in a binary format, are converted to CITVAP format by the interface package; BORGES.

Using these codes to generate initial flux for calculations increases the accuracy of outputs to represent the reality of phenomenon. In addition, taking fuel burn up into account as well as different feedbacks including temperatures, xenon, and samarium along with boron concentration results in accurate time dependent neutron density and power changes. Considering fuel burn up to use accurate time dependent delayed neutron fraction instead of assuming an average value in previous works and using variable fuel and coolant temperature reactivity coefficients, increase the results accuracy.

Because of the reactivity insertion transients have attracted much attention (Bousbia Salah and Hamidouche, 2005), (El-Messiry, 2000), (Hany et al., 2007), (Kazeminejad, 2006), and (Gaheen et al., 2007) the model is successfully applied to generate the steady state and the kinetic and dynamic behaviors under reactivity insertion transient of Tehran pool type research reactor core. Section 2 describes model for the reactor under consideration with representing different concept included. In Section 3, we consider steady state and reactivity insertion transient with a comparison with experimental data and RELAP5/Mod3. Conclusions are drawn based on results and discussions in section 4.

2. Reactor model

In this work, a thirty fourth order model is used to simulate the kinetics and dynamics of a research reactor. The model assumes point kinetics equations with six delayed neutron groups, temperature feedbacks from lumped fuel and coolant temperatures with variable reactivity coefficients, xenon and samarium effects, fuel burn up and boron concentration. The model can be used for power reactors to simulate dynamics behavior. Also, the model coupled with WIMS and CITVAP codes at input for more accurate initial neutron flux which is used for burn up calculations. The underlying concepts for deriving the model are presented in the rest of paper.

2.1. Thermal hydraulic model

Consider a typical pool-type research reactor with MTR-type fuel elements of rectangular geometry, cooled and moderated with light water. A one-dimensional core is considered, consisting of a cooling channel of width 2b and a fuel plate of width 2d. Incompressible slug flow of velocity U is assumed to take place in the channel, whereas convective heat transfer is assumed to take place on the plate surface through a constant heat transfer coefficient h. Based on (Housiadas, 2002) and doing an energy balance on a lumped model for the fuel and clad using Newton's law of cooling, the fuel temperature is obtained. Performing a time-dependent energy balance on the reactor core using the conservation of energy, the equations for the local coolant temperature $\hat{T}_C$ and fuel temperature $\hat{T}_f$ are as follows:

$$\rho_c c_c \frac{\partial \hat{T}_C}{\partial t} + \rho_c c_c U \frac{\partial \hat{T}_C}{\partial z} = \frac{h}{b}\left(\hat{T}_f - \hat{T}_C\right) \quad (1)$$

$$\rho_f c_f \frac{d\hat{T}_f}{dt} = -\frac{h}{d}\left(\hat{T}_f - \hat{T}_C\right) + \hat{P} \quad (2)$$

Local power density is assumed to have the profile of the fundamental eigenfunction (cosine form). The mean (core-averaged) value of an axially dependent quantity like $\hat{T}_C$ is given by

$$T_c(t) = \frac{1}{H}\int_0^H \hat{T}_C(z,t)dz \quad (3)$$

By applying the above rule on both sides of equations (1) and (2), one obtains

$$\rho_c c_c \frac{\partial T_c}{\partial t} + \rho_c c_c \frac{U}{H}\left(T_{out} - T_p\right) = \frac{h}{b}\left(T_f - T_c\right) \quad (4)$$

$$\rho_f c_f \frac{dT_f}{dt} = -\frac{h}{d}\left(T_f - T_c\right) + P_0 \quad (5)$$

In agreement with the point kinetics model, assume that the shape of functions $\hat{T}_C(z,t)$ and $\hat{T}_f(z,t)$ remains unchanged with time, and identical to the profile corresponding to static conditions. Considering the steady-state solutions of equations (1) and (2) it can be shown that the axial profiles can be expressed as follows

$$\hat{T}_C = T_p + (T_c - T_p)\left[1 - \cos\left(\frac{\pi z}{H}\right)\right] \quad (6)$$

$$\hat{T}_f = T_p + \left(T_c - T_p\right)\left[1 - \cos\left(\frac{\pi z}{H}\right)\right] + \frac{\pi}{2}(T_f - T_c)\sin\left(\frac{\pi z}{H}\right) \quad (7)$$

The above expressions permit to approximate the axial temperature distributions of coolant and fuel element with the help of the mean temperatures T_c and T_f, i.e. the lumped parameters. More specifically, equation (6) permits to write

$$T_c = (T_{out} + Tp)/2 \quad (8)$$

which enables equation (1) to be expressed in terms of the lumped parameters T_c and T_f as follows

$$\rho_c c_c \frac{dT_c}{dt} + 2\rho_c c_c \frac{U}{H}(T_c - T_p) = \frac{h}{b}(T_f - T_c) \quad (9)$$

On the other hand, equation (7) can be used to determine the maximum fuel temperature point. By differentiating equation (7) with respect to z, equating to zero, and solving for z, it follows that the axial location at which the maximum fuel temperature occurs is

$$z_m = \frac{H}{2} + \frac{H}{\pi}\tan^{-1}\frac{2}{\pi}\frac{T_c - T_p}{T_f - T_c} = \frac{H}{2} + \frac{H}{\pi}tan^{-1}\frac{hH}{\pi\rho_c c_c Ubd} \quad (10)$$

In the present simulations the heat transfer coefficient is determined from the Dittus–Boelter correlation for turbulent-flow convection. The core inlet temperature (or pool temperature) T_p is normally a constant specified as an input parameter. However, the option of pool heating has been also accommodated to analyze conditions in which pool temperature rises because of simultaneous loss of secondary cooling. This can be accomplished by introducing an additional differential equation, based on a simple heat balance over the pool volume

$$\rho_c c_c V_P \frac{dT_P}{dt} = V_f P \quad (11)$$

2.2. Point reactor kinetics model

The neutron density and delayed precursor concentrations are obtained from the following equations

$$\frac{d}{dt}n(t) = \frac{[\rho(t) - \beta(t)]n(t)}{\Lambda} + \sum_{i=1}^{N}\lambda_i C_i(t) + Q \quad (12)$$

$$\frac{d}{dt}C_i(t) = \frac{\beta_i}{\Lambda}n(t) - \lambda_i C_i(t) \qquad i = 1, 2, \ldots, 6 \quad (13)$$

The point kinetics equations are uncommon with respect to units. Both reactivity and the delayed neutron fraction are unitless. The delayed neutron fraction is the fraction of the total neutrons resulting from a fission that are not emitted instantaneously (delayed neutrons per total neutrons).

The only terms in the point kinetics equations with absolute physical units are Λ and λ, which have units of time and inverse time, respectively. In order for the equations to be dimensionally consistent n and C must have the same units, while Q must have units of dn/dt. The point kinetics equations are derived from diffusion or transport theory–equations that describe the neutron population (Bell and Glasstone, 1970; Duderstadt and Hamilton, 1976). The units of n and C must then be n/cm3 (a density since the point kinetics equations are 0-D) or any quantity directly proportional to this. In a one-neutron energy group model, the neutron speed v is a constant and therefore the neutron flux, given below in Equation (14), is always directly proportional to the neutron population n. This allows the point kinetics equations to be cast in terms of the neutron flux. This is a convenient form of the point kinetics equations as flux is also used to calculate reaction rates. For this reason the point kinetics equations are coded in the form given by Equations (15) and (16).

$$\phi(t) = vn(t) \quad (14)$$

$$\frac{d}{dt}\phi(t) = \frac{[\rho(t) - \beta(t)]\phi(t)}{\Lambda} + \sum_{i=1}^{N}\lambda_i C_i(t) + Q \quad (15)$$

$$\frac{d}{dt}C_i(t) = \frac{\beta_i}{\Lambda}\phi(t) - \lambda_i C_i(t) \qquad i = 1, 2, \ldots, 6 \quad (16)$$

However, for reactor operating in the critical state with steady output power, the effect of external source can be neglected.

Reactivity ρ(t) is determined by calculating continuous reactor feedback as follows

$$\rho(t) = \delta\rho_r + \delta\rho_b + \alpha_f(T_f, T_c)(T_f - T_{f0}) + \alpha_c(T_f, T_c)(T_c - T_{c0}) - \sigma_X(X - X_0) - \sigma_S(S - S_0) \quad (17)$$

In the above expression, the first two terms in the right-hand side are the externally introduced reactivity (i.e., reactivity due to control rod insertion introduced in the model by $\frac{d\delta\rho_r}{dt} = G_r z_r$ and change of the boron concentration introduced in the model by $\frac{d\delta\rho_b}{dt} = B_r v_r$, boron concentration reactivity coefficient characterizes the reaction of the core to boron absorber content variation in the coolant) and the remaining terms are the various feedback contributions.

Feedback effects are induced by changes of coolant temperature T_c, changes of fuel temperature T_f (Doppler effects), changes of xenon concentration $\sigma_X(X - X_0)$, and changes of samarium concentration $\sigma_S(S - S_0)$.

Reactivity coefficients characterize the reaction of the core to variation of operating parameters. Fuel temperature reactivity coefficient represents fuel temperature reactivity derivative at other constant parameters (coolant temperature and density, boron concentration, xenon poisoning, burn-up etc.). Coolant (moderator) temperature reactivity coefficient represents a coolant temperature reactivity derivative taking into account the corresponding variation of coolant density at other constant parameters (fuel temperature, boron concentration, xenon poisoning, burn-up etc.).

Temperature increase results in coolant density decrease, which causes decreasing of moderator atoms quantity in the unit of volume and reactivity decreasing. With boron presence the volume content of boron absorber will also decrease in the coolant. With sufficiently high values of boron concentration a positive contribution to temperature reactivity coefficient connected with relative decrease of neutron absorption can be dominant.

The least negative values of temperature reactivity coefficient are realized at reactor start-up at the beginning of fuel cycles when critical

concentration of boric acid in the coolant is at the highest. The most negative values of temperature reactivity coefficient occur at the end of fuel cycles with decrease of boric acid concentration to practically zero value. So, it is clear that variable reactivity coefficient should be use in model to better simulating the dynamics of reactor.

The corresponding coefficients of reactivity due to fuel and coolant are $\alpha_f(T_f, T_c)$, $\alpha_c(T_f, T_c)$ respectively. Equation (17) implies that there are variable reactivity coefficients (i.e., the current model does incorporate temperature of fuel and coolant dependence into the fuel and moderator temperature feedback coefficients) which can introduce less simplification into the model resulting in more reality and such approach is applicable to transient cases. So, the slopes $\frac{\partial \rho}{\partial T_f}$ and $\frac{\partial \rho}{\partial T_c}$ are taken into account instead of being taken constant over extended ranges of variation for parameters T_c and T_f. This can be achieved by introducing a lookup table of different reactivity schemes in SAR (SARforTRR, 2002) of research reactor and defining a simple interpolation scheme such as RELAP approach instead of entering differential equations in the model.

Additional time dependence in any of the parameters in Equations (15) and (16) due to longer-term changes in fuel composition will be discussed in the next subsection on time dependent delayed neutron fraction.

2.3. Time dependent delayed neutron fraction (burn up calculations)

During the operation of a nuclear reactor a number of changes occur in the composition of the fuel. The various fuel nuclei are transmuted by neutron capture and subsequent decay. For a uranium fueled reactor, this process produces a variety of transuranic elements in the actinide series of the periodic table. The fission event destroys a fissile nucleus, of course, and in the process produces two intermediate mass fission products. The fission products tend to be neutron-rich and subsequently decay by beta or neutron emission (usually accompanied by gamma emission) and undergo neutron capture to be transmuted into a heavier isotope, which itself undergoes radioactive decay and neutron transmutation, and so on. The fissile nuclei also undergo neutron transmutation via radiative capture followed by decay or further transmutation. Transmutation–decay chains for ^{238}U are shown in Fig. 1.

Based on (Stacey, 2007) for reactors operating on the uranium cycle, the isotopic concentrations are described by

$$\frac{dn^{24}}{dt} = -\sigma_a^{24}\phi n^{24} \quad (18)$$

$$\frac{dn^{25}}{dt} = \sigma_\gamma^{24}\phi n^{24} - \sigma_a^{25}\phi n^{25} \quad (19)$$

$$\frac{dn^{26}}{dt} = \sigma_\gamma^{25}\phi n^{25} - \sigma_a^{26}\phi n^{26} + \lambda_{ec}^{36}\phi n^{36} \quad (20)$$

$$\frac{dn^{27}}{dt} = \sigma_\gamma^{26}\phi n^{26} + \sigma_{n,2n}^{28}\phi n^{28} - \lambda^{27}\phi n^{27} \quad (21)$$

$$\frac{dn^{28}}{dt} = -\sigma_a^{28}\phi n^{28} \quad (22)$$

$$\frac{dn^{29}}{dt} = \sigma_\gamma^{28}\phi n^{28} - (\lambda^{29} + \sigma_a^{29}\phi)n^{29} \quad (23)$$

$$\frac{dn^{36}}{dt} = \sigma_{n,2n}^{37}\phi n^{37} - (\lambda^{36} + \sigma_a^{36}\phi)n^{36} \quad (24)$$

$$\frac{dn^{37}}{dt} = \lambda^{27}n^{27} - \sigma_a^{27}\phi n^{27} \quad (25)$$

$$\frac{dn^{38}}{dt} = \sigma_\gamma^{37}\phi n^{37} - (\lambda^{38} + \sigma_a^{38}\phi)n^{38} \quad (26)$$

$$\frac{dn^{39}}{dt} = \lambda^{29}n^{29} - (\lambda^{39} + \sigma_a^{39}\phi)n^{39} \quad (27)$$

$$\frac{dn^{48}}{dt} = \lambda^{38}n^{38} - \sigma_a^{48}\phi n^{48} \quad (28)$$

$$\frac{dn^{49}}{dt} = \lambda^{39}n^{39} - \sigma_a^{49}\phi n^{49} + \sigma_\gamma^{48}\phi n^{48} \quad (29)$$

$$\frac{dn^{40}}{dt} = \sigma_\gamma^{49}\phi n^{49} - \sigma_a^{40}\phi n^{40} + \sigma_\gamma^{29}\phi n^{29} + \sigma_\gamma^{39}\phi n^{39} \quad (30)$$

$$\frac{dn^{41}}{dt} = \sigma_\gamma^{40}\phi n^{40} - (\lambda^{41} + \sigma_a^{41}\phi)n^{41} \quad (31)$$

$$\frac{dn^{42}}{dt} = \sigma_\gamma^{42}\phi n^{42} - (\lambda^{43} + \sigma_a^{43}\phi)n^{43} \quad (32)$$

$$\frac{dn^{51}}{dt} = \lambda^{41}n^{41} - (\lambda^{51} + \sigma_a^{51}\phi)n^{51} \quad (33)$$

$$\frac{dn^{52}}{dt} = \sigma_\gamma^{51}\phi n^{51} - \sigma_a^{52}\phi n^{52} \quad (34)$$

$$\frac{dn^{53}}{dt} = \lambda^{43}n^{43} - \sigma_a^{53}\phi n^{53} + \sigma_\gamma^{52}\phi n^{52} \quad (35)$$

Fig. 2 shows the results of simultaneous solving of these equations. As expected, delayed neutron fraction decreases with increasing burn up; this is because the delayed neutron fraction of ^{239}PU is smaller than the fraction of delayed neutron of ^{235}U.

Now in each time step the isotopic composition of fuel is known, so it is possible to calculate reactivity and time dependent delayed neutron fraction in each time step.

Reactivity is calculated using (k-1)/k, so k_{eff} should be calculated first by

$$k_{eff}(t) = \frac{\nu\Sigma_f(t)}{\Sigma_a(t)(1+L^2B^2)} = \frac{\sum_{i=1}^{17}\nu_i\sigma_{f,i}N_i(t)}{(1+L^2B^2)[\sum_{i=1}^{17}N_i\sigma_{a,i}]+ X\sigma_X+S\sigma_S+F*\sigma_a^{fission}+ N_{water}\sigma_a^{water}+N_{boron}\sigma_a^{boron}} \quad (36)$$

In this equation, $\left[\sum_{i=1}^{17} N_i\, \sigma_{a,i}\right]$ is a sum over the absorption cross sections due to the actinides. $X\sigma_X$ and $S\sigma_S$ calculate the absorption cross sections of 135Xe and 149Sm. $F * \sigma_a^{fission}$ approximates absorption for all other fission products. The total number of fissions, F, that have occurred in the fuel since the beginning of irradiation and can be calculated using

$$\frac{dF}{dt} = \phi(t)\sum_{i=1}^{17} N_i\, \sigma_f^i \quad (37)$$

According to (Tashakor et al., 2010) and (Matthew Johnson et al., 2010), Isotopic composition of fuel enable us to calculate time dependent delayed neutron fraction. As stated, changes in the elements concentrations may be written as $\frac{dn}{dt} = P - L$, where

P is the production rate and L is the consumption or leakage rate. For fissile material, the isotopes that are considered are ^{235}U, ^{239}Pu, and ^{238}U. The delayed neutron fraction for each delayed neutron group is calculated using

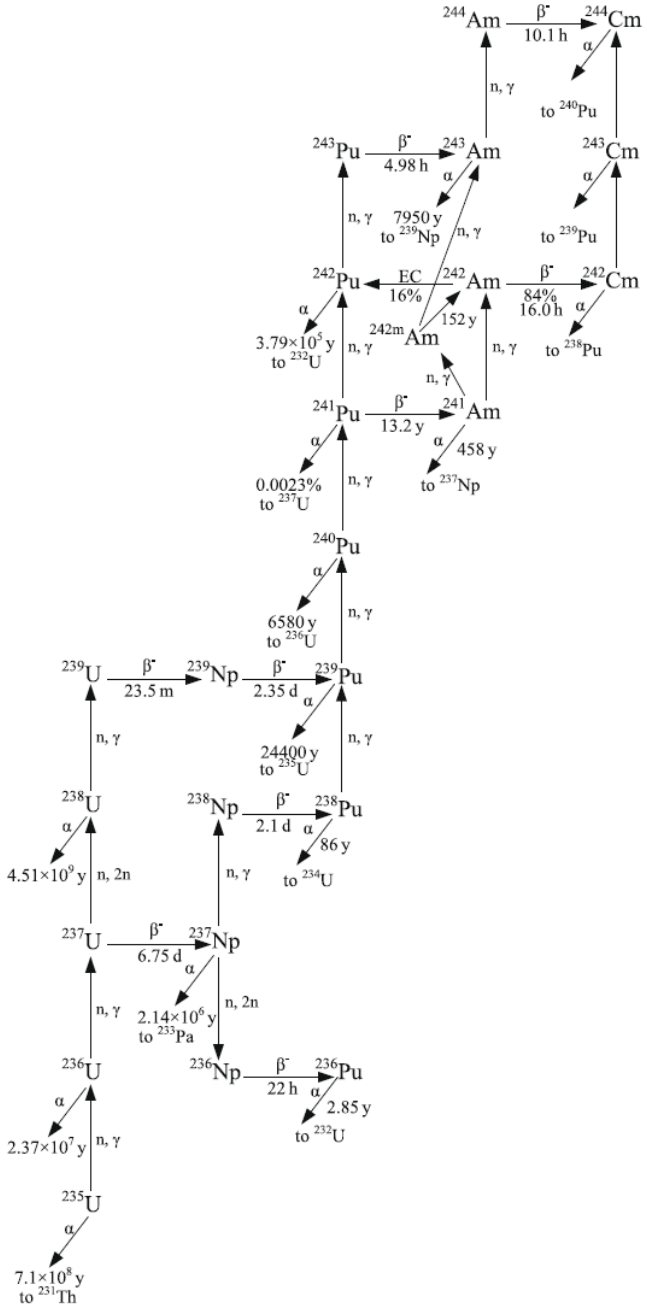

Fig. 1: Transmutation–decay chains for 238U (Benedict et al., 1981)

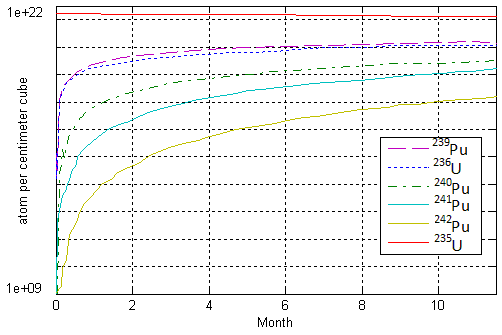

Fig. 2: Output of solving depletion equations

$$\beta^{i} = \frac{\sum_{j=1}^{3} \nu_j \sigma_f^j N_j(t) \beta_j^i}{\sum_{j=1}^{3} \nu_j \sigma_f^j N_j(t)} \quad (38)$$

Fig. 3 shows the changes in the six-group delayed neutron fraction as a function of time. In fact, at reactor start up time, ^{238}U has about 14.6% of the fission contribution spectrum and ^{235}U about 85.4%. Thus the fraction of delayed neutrons for uranium fuel (0.027 weight fraction ^{235}U in U) at reactor start up time is about 0.0085 for six-group delayed neutron precursor versus 0.00771 for one-group.

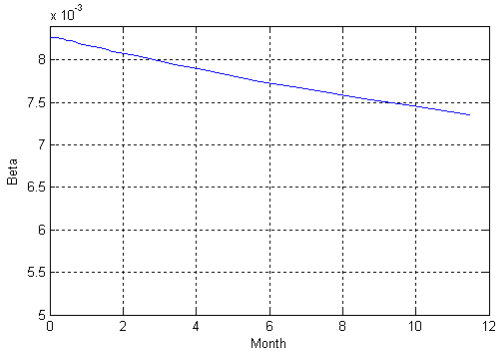

Fig. 3: The dependent delayed neutron fraction in a fuel cycle

2.4. Reactor model equations

The model can be summarized as follows:

$$\frac{d}{dt}\phi(t) = \frac{[\rho(t)-\beta(t)]\phi(t)}{\Lambda} + \sum_{i=1}^{N} \lambda_i C_i(t) \quad (39)$$

$$\frac{d}{dt}C_i(t) = \frac{\beta_i}{\Lambda}\ \phi(t) - \lambda_i C_i(t) \qquad i = 1, 2, \ldots, 6 \quad (40)$$

$$\rho_c c_c \frac{\partial T_c}{\partial t} + \rho_c c_c \frac{U}{H}\left(T_{out} - T_p\right) = \frac{h}{b}\left(T_f - T_c\right) \quad (41)$$

$$\rho_f c_f \frac{dT_f}{dt} = -\frac{h}{d}\left(T_f - T_c\right) + P_0 \quad (42)$$

$$\rho_c c_c V_P \frac{dT_P}{dt} = V_f P \quad (43)$$

$$\frac{dF}{dt} = \phi(t) \sum_i N_i \sigma_f^i \quad (44)$$

$$\frac{d\delta\rho_b}{dt} = B_r v_r \quad (45)$$

$$\frac{d\delta\rho_r}{dt} = G_r z_r \quad (46)$$

$$\frac{dP}{dt} = \gamma^{Nd} \sum_f \phi(t) - \lambda^P P \quad (47)$$

$$\frac{dS}{dt} = \lambda^P P - \sigma_a^S \phi(t) S \quad (48)$$

$$\frac{dI}{dt} = \gamma^I \sum_f \phi(t) - \lambda^I I \quad (49)$$

$$\frac{dX}{dt} = \lambda^X \sum_f \phi(t) + \lambda^I I - \left(\lambda^X + \sigma_a^X \phi(t)\right) X \quad (50)$$

$$\rho(t) = \delta\rho_r + \ \delta\rho_b + \alpha_f(T_f,\ T_c)\left(T_f - T_{f0}\right) + \alpha_c(T_f, T_c)(T_c - T_{c0}) - \sigma_X(X - X_0) - \sigma_S(S - S_0) \quad (51)$$

$$\frac{dn^{24}}{dt} = -\sigma_a^{24} \phi n^{24} \quad (52)$$

$$\frac{dn^{25}}{dt} = \sigma_\gamma^{24} \phi n^{24} - \sigma_a^{25} \phi n^{25} \quad (53)$$

$$\frac{dn^{26}}{dt} = \sigma_\gamma^{25} \phi n^{25} - \sigma_a^{26} \phi n^{26} + \lambda_{ec}^{36} \phi n^{36} \quad (54)$$

$$\frac{dn^{27}}{dt} = \sigma_\gamma^{26} \phi n^{26} + \sigma_{n,2n}^{28} \phi n^{28} - \lambda^{27} \phi n^{27} \quad (55)$$

$$\frac{dn^{28}}{dt} = -\sigma_a^{28} \phi n^{28} \quad (56)$$

$$\frac{dn^{29}}{dt} = \sigma_\gamma^{28} \phi n^{28} - (\lambda^{29} + \sigma_a^{29} \phi) n^{29} \quad (57)$$

$$\frac{dn^{36}}{dt} = \sigma_{n,2n}^{37} \phi n^{37} - (\lambda^{36} + \sigma_a^{36} \phi) n^{36} \quad (58)$$

$$\frac{dn^{37}}{dt} = \lambda^{27} n^{27} - \sigma_a^{27} \phi n^{27} \quad (59)$$

$$\frac{dn^{38}}{dt} = \sigma_{\gamma}^{37}\phi n^{37} - (\lambda^{38} + \sigma_a^{38}\phi)n^{38} \quad (60)$$

$$\frac{dn^{39}}{dt} = \lambda^{29}n^{29} - (\lambda^{39} + \sigma_a^{39}\phi)n^{39} \quad (61)$$

$$\frac{dn^{48}}{dt} = \lambda^{38}n^{38} - \sigma_a^{48}\phi n^{48} \quad (62)$$

$$\frac{dn^{49}}{dt} = \lambda^{39}n^{39} - \sigma_a^{49}\phi n^{49} + \sigma_{\gamma}^{48}\phi n^{48} \quad (63)$$

$$\frac{dn^{40}}{dt} = \sigma_{\gamma}^{49}\phi n^{49} - \sigma_a^{40}\phi n^{40} + \sigma_{\gamma}^{29}\phi n^{29} + \sigma_{\gamma}^{39}\phi n^{39} \quad (64)$$

$$\frac{dn^{41}}{dt} = \sigma_{\gamma}^{40}\phi n^{40} - (\lambda^{41} + \sigma_a^{41}\phi)n^{41} \quad (65)$$

$$\frac{dn^{42}}{dt} = \sigma_{\gamma}^{42}\phi n^{42} - (\lambda^{43} + \sigma_a^{43}\phi)n^{43} \quad (66)$$

$$\frac{dn^{51}}{dt} = \lambda^{41}n^{41} - (\lambda^{51} + \sigma_a^{51}\phi)n^{51} \quad (67)$$

$$\frac{dn^{52}}{dt} = \sigma_{\gamma}^{51}\phi n^{51} - \sigma_a^{52}\phi n^{52} \quad (68)$$

$$\frac{dn^{53}}{dt} = \lambda^{43}n^{43} - \sigma_a^{53}\phi n^{53} + \sigma_{\gamma}^{52}\phi n^{52} \quad (69)$$

3. Solution recipe

Because of point kinetic equations are stiff in nature; a numerical solution should be selected to guarantee the solution. After testing different numerical methods such as Euler, Runge – Kutta, etc, we came to decision of using MATLAB ode suit. For this reason ODE15s function of MATLAB is used to solve the model which is able to efficiently solve stiff problems. Variable order solver based on the numerical differentiation formulas (NDFs); ode15s optionally uses the backward differentiation formulas, BDFs (also known as Gear's method (Gear, 1971)). Matlab's NDFs are more accurate than the BDFs, but at higher orders are slightly less stable. For each time-step, the new time value of the solution is solved for using chord iteration. If user-defined error tolerances cannot be met, the solver will adjust the time step size and re-attempt to find a solution. If desired, the user can set the maximum order of the formulae used and whether to use the BDFs instead of the NDFs. The background of ODE solver in MATLAB is based on researches such as (Bank et al., 1985; Bogacki and L. F. Shampine, 1989; Dormand and Prince, 1980; Forsythe et al., 1977; Kahaner et al., 1989; Shampine, 1994; Shampine and Gordon, 1975; Shampine and Hosea, 1996; Shampine et al., 1999; Shampine and Reichelt, 1997). Other researchers have taken similar approaches (Matthew Johnson et al., 2010; Wang et al., 2011).

Indeed, The BDF's are very popular for solving stiff problems. When the step size is a constant h and backward differences are used, the formula of order k, BDFk, for a step from (t_n, y_n) to (t_{n+1}, y_{n+1}) is

$$\sum_{m=1}^{k} \frac{1}{m}\nabla^m y_{n+1} - hF(t_{n+1}, y_{n+1}) = 0 \quad (70)$$

The algebraic equation for y_{n+1} is solved with a simplifed Newton (chord) iteration. The iteration is started with the predicted value

$$y_{n+1}^{(0)} = \sum_{m=0}^{k} \nabla^m y_n \quad (71)$$

The leading term of the BDFk truncation error can be conveniently approximated as

$$\frac{1}{k+1}h^{k+1}y^{k+1} \approx \frac{1}{k+1}\nabla^{k+1}y_{n+1} \quad (72)$$

The typical implementation of a general-purpose BDF code is quasi-constant step size. This means that the formulas used are those for a constant step size and the step size is held constant during an integration unless there is good reason to change it. General-purpose BDF codes also vary the order during an integration. Noting that the predictor (71) has a longer memory than (70), (Klopfenstein, 1971) considered how to exploit this to obtain better stability. Klopfenstein studied methods of the form

$$\sum_{m=1}^{k} \frac{1}{m}\nabla^m y_{n+1} - hF(t_{n+1}, y_{n+1}) - \kappa\gamma_k(y_{n+1} - {y_{n+1}}^0) = 0 \quad (73)$$

that he called numerical differentiation formulas, NDF's. Here κ is a scalar parameter and the coefficients γ_k are given by $\gamma_k = \sum_{j=1}^{k} \frac{1}{j}$. The role of the term added to BDFk is illuminated by the identity

$$y_{n+1} - {y_{n+1}}^0 = \nabla^{k+1}y_{n+1}$$

and the approximation (72) to the truncation error of BDFk. It follows easily that for any value of the parameter κ, the method is of order (at least) k and the leading term of its truncation error is

$$(\kappa\gamma_k + \frac{1}{k+1})h^{k+1}y^{k+1} \quad (74)$$

For orders 3-6, Klopfenstein found numerically the κ that maximizes the angle of A(α)-stability. Because BDF2 is already A-stable, Klopfenstein considered how to choose κ so as to reduce the truncation error as much as possible whilst still retaining A-stability. The optimal choice is $= -1/9$, yielding a truncation error coefficient half that of BDF2. This implies that for sufficiently small step sizes, NDF2 can achieve the same accuracy as BDF2 with a step size about 26% bigger.

The formulas derived by Klopfenstein at orders higher than 2 are less successful because the price of improved stability is reduced efficiency. Taking the opposite tack, we sought values of κ that would make the NDF's more accurate than the BDF's and not much less stable. Of course the leading term of the truncation error cannot be made too small, else it would not dominate and the formula would not behave as expected at realistic step sizes. Because Klopfenstein's second order formula optimally improves accuracy while retaining L-stability, it serves as the order 2 method of our NDF family. Correspondingly, we sought to obtain the same improvement in efficiency (26%) at orders 3-5. This comes at the price of reduced stability and we were not willing to reduce the stability angle by more than 10%. The search was carried out numerically. Our choices and the compromises made in balancing

efficiency and stability are shown in Table 1. The stability of BDF5 is so poor that we were not willing to reduce it at all.

Regarding comparison between ODE15s and ODE45, power upgrading was selected to compare them (as discussed in (Wang et al., 2011)). Result showed that the power response results, which are calculated respectively by the general differential equation solver Ode45 with 0.01 s as the max simulation step size and by the stiff equation solver Ode15s with the automatic selection simulation step size are in accord well with each other, which shows that the stiff equation solver Ode15s with the automatic selection simulation step size can obtain the satisfactory precision. In 900 simulated seconds, the general differential equation solver Ode45s needs to calculate 90012 steps in all with the minimal simulation step size 6.2713e-5 second, and the computer consumes 14.68 s.

Table 1: The Klopfenstein-Shampine NDF's and their efficiency and A(α)-stability relative to the BDF's

Order k	NDF Coeff. κ	Step ratio percent	stability angle		Percent change
			BDF	NDF	
1	-0.1850	26%	90°	90°	0%
2	-1.9	26%	90°	90°	0%
3	-0.0823	26%	86°	80°	-7%
4	-0.0415	12%	73°	66°	-10%
5	0	0%	51°	51°	0%

However, the stiff equation solver Ode15s only needs 0.12 s to calculate 832 steps in all with the maximal simulation step size 11.1326 s. It can be found that the solver Ode15s is suitable for solving the stiff equation and can automatically adjust the calculation step size according to the real variation of power. Thus, the solver Ode15s can be employed to perform the quick calculation even pre-real time forecast of the response to load variation for the operators in the operating field.

In this method first the reactor core should be modeled in WIMS, BORGES, and CITVAP using MTR_PC code to generate general flux using transport equation, extracting cross sections, and initial average flux using diffusion equations and then initial values such as reactivity feedback lookup table, kinetic parameters, and etc., are prepared for running thirty fourth order dynamic model. It is worth mentioning that in each time step, neutron flux is calculated and fed to Bateman equations part of the model to calculate burn up in that time step.

4. Results and discussions

The model is successfully applied to generate the steady state and the kinetic and dynamic behaviors under reactivity insertion transient of Tehran pool type research reactor core. Tehran research reactor (TRR) is a 5 MW pool type research reactor located in Tehran. This reactor consists of MTR low enriched uranium (LEU) fuel type. The reactor core is cooled by downward forced flow of light water circulated by a primary cooling circuit pump during the normal operational stage. Its main components are reactor core, control and safety systems, pool, holdup tank, pumps, heat exchanger, connecting pipes, check valves, gate valves and butterfly valves. Some of the main reactor data are outlined in Table 2 and detailed specifications data are given in (Barati and Setayeshi, 2012, 2013). Also, Fig. 4 shows the core configuration which have been used in this study.

4.1. Steady state

In developing dynamic models it is common to test the model in steady state mode with proven or experimental data to be sure that the model is working well. Then accidents are modeled and validated with other experiments and codes. For this reason, results from steady state experimental data of Tehran research reactor are used for comparison. The results of this comparison are shown in Table 3 and there is a good agreement in results. It should be noted that at steady state, when time is zero t=0 all time derivatives are equal to zero, all d/dt=0 and the initial value of the relative power equals unity n(0)=1, and also no reactivity perturbation is present $\delta k = 0$.

$$n(0) = 0, \frac{dn}{dt} = 0, \delta k = 0, \sum_{i=1}^{6} \lambda_i C_i = \frac{\beta}{\Lambda}, \frac{dC_i}{dt} = 0, C_{i0} = \frac{\beta_i}{l\boldsymbol{\lambda_i}}$$

4.1. Reactivity insertion for Tehran research reactor

This type of accident is specified by a rapid transient governed by the core kinetics, and strong interactions between the kinetics and thermal–hydraulics are involved.

For a research reactor, reactivity insertion events may occur during the refueling or the unexpected withdrawing of the control rod. These events are considered one of the most severe accidents that could lead to core damage, because during such events the core become supercritical and the core power rises to level beyond the heat removal system's capability.

Two categories of reactivity insertions are taken into account; fast reactivity insertion (1.5 $/0.5s) and slow reactivity insertion (0.09 $/1.0s) at BOC. Definitions of transients are presented in Table 4.

In FRIA simulation, it has been assumed that all the protection and safety circuits fail except the overpower trip at 120% nominal power. A delay

time of 25 ms was considered between trip level and start of shutdown reactivity insertion (-10$/0.5 s). Results of both SRIA and FRIA are presented in Fig. 5 to Fig. 12. Also, based on similar works in validation (March - Leuba, 1986; Espinosa-Paredes and Álvarez-Ramírez, 2003; Nuñez-Carrera et al., 2004; Espinosa-Paredes et al, 2004; Espinosa-Paredes and Nuñez-Carrera, 2008; Espinosa-Paredes and Espinosa-Martínez, 2009; Espinosa-Paredes et al., 2012) a comparison with RELAP, PARET and TRR SAR is presented in Table 5 for validation purposes. In this comparison, the kinetics parameters (reactivity coefficients, delayed neutron parameters) are the same for the other codes as used in the 34th order model.

This model of accident shows that the peak fuel temperature is smaller than the aluminum melting temperature (630 ℃) so these is no core melt down.

It can be seen that the FRIA and SRIA transients have a similar shape. Because of the positive reactivity insertion, the power increased rapidly, which resulted in the temperature increase of the fuel meat, clad and coolant in sequence. With 25 ms delay after the power exceed 6 MW, all these parameters decreased because of the scram.

Table 2: Specifications and main operating conditions of Tehran research reactor

Core material	
Coolant	Light water
Fuel element	Plate-type clad in Al
Moderator	Light water
Nuclear fuel	MTR (LEU)
Reflector	Graphite/light water
Thermo-hydraulics	
Cladding thermal conductivity (W/m K)	167.0
Cooling method	Forced flow
Fuel thermal conductivity (W/m K)	10.0
Holdup tank water volume (m3)	37.417
Inlet coolant temperature (°C)	37.8
Pool water volume (m3)	477.8
Fuel element dimensions	
Fuel height (cm)	70.5
Fuel length (cm)	8.1
Fuel width (cm)	7.07
Number of plates in standard fuel elements	19
Passing cooling water cross-section (cm2) at (CFE)	25.81
Fuel meat	
^{235}U (%)	12.44
^{238}U (%)	49.78
O (%)	11.17
Al (%)	26.50

Table 3: A comparison between the results of simulation and the experimental data (SARforTRR, 2002)

Temperature	Results of the proposed model	Data Registered at SAR
Pool outlet Temperature (°C)	**37.8**	**37.8**
Pool Inlet Temperature (°C)	**48.9**	**49.1**

Table 4: Definition of transients in TRR with scram (BOC)

Transient key parameters	RIA
Initial Power	**1e-9 MW**
Rate of external positive reactivity addition	**1.5 $/0.5 s (fast RIA)**
	0.09 $/1.0 s (slow RIA)
β_{eff}	**0.008303**
Λ (μs)	**33.8280**
Coolant temperature feedback coefficient (1/K)	**7.96e-3**
Fuel temperature coefficient (1/K)	**2.13e-3**
Scram setting point	**(120% of nominal power)**
Delay time before scram (ms)	**25**
Shut down reactivity	**-10$/0.5 s**

Table 5: Code validation based on the RIA

	Presented model	RELAP5/Mode3.2	PARET	Data registered at TRR SAR
Slow reactivity insertion accident ($0.09/1.0s)				
Trip time (s)	**10.59**	**10.62**	**10.62**	**---**
Peak power (MW)	**10.50**	**10.40**	**10.38**	**---**
Peak Temperature (°C)				
Fuel	**67.00**	**69.50**	**71.00**	**---**
Coolant	**48.20**	**50.00**	**49.00**	**---**
Fast reactivity insertion accident ($1.5/0.5s)				
Trip time (s)	**0.61**	**0.62**	**0.60**	**0.60**
Peak power (MW)	**100.00**	**101.00**	**99.00**	**99.80**
Peak Temperature (°C)				
Fuel	**155.40**	**158.00**	**157.00**	**156.00**
Coolant	**68.70**	**70.00**	**71.00**	**69.00**

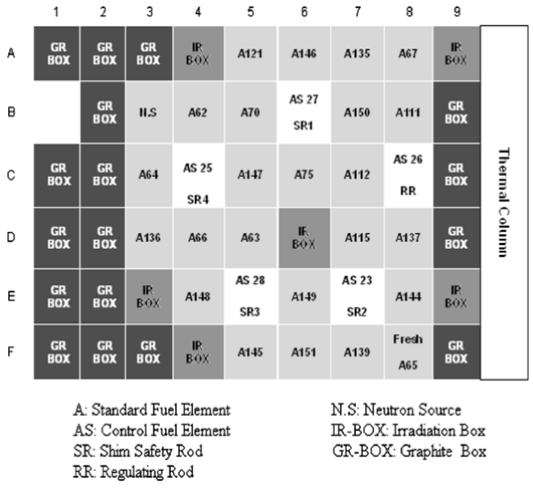

Fig. 4: TRR core configuration

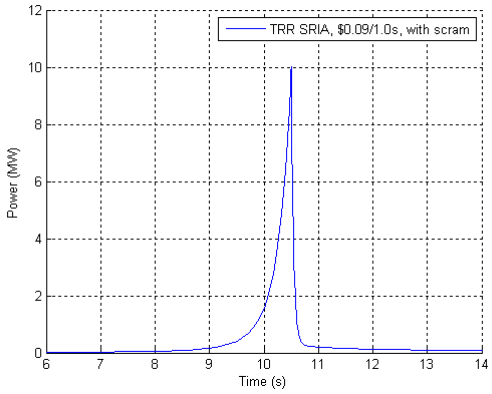

Fig. 5: TRR power response as a function of time in SRIA

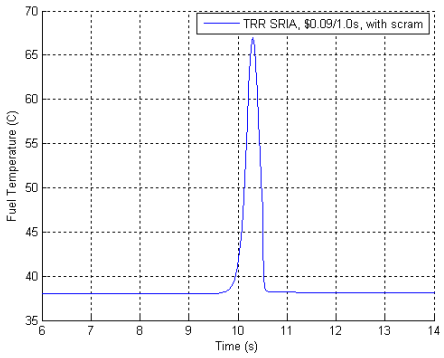

Fig. 6: Changes in fuel temperature as a function of time in SRIA

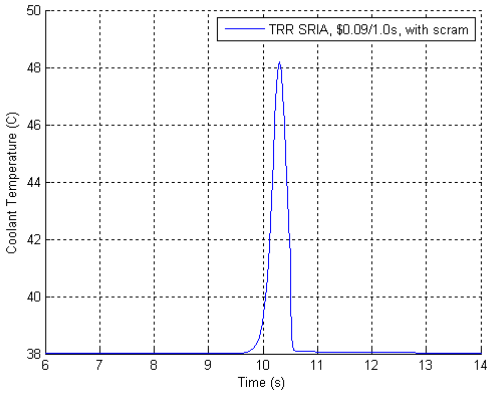

Fig. 7: Changes in coolant temperature as a function of time in SRIA

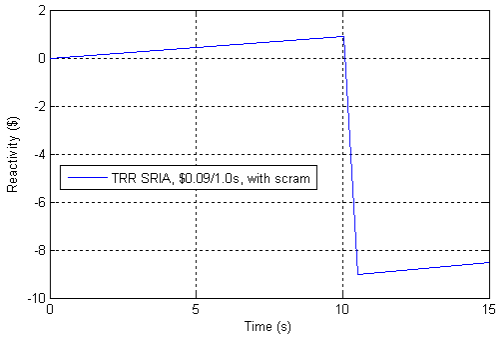

Fig. 8: Changes in reactivity as a function of time in SRIA

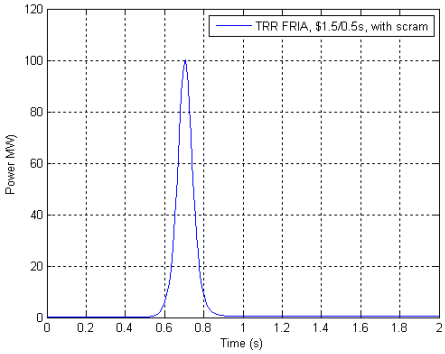

Fig. 9: TRR power response as a function of time in FRIA

However, there were some differences between the FRIA and the SRIA. The core power almost rose to as large as 100MW quickly in the FRIA, which was much larger than that (10 MW) in the SRIA.

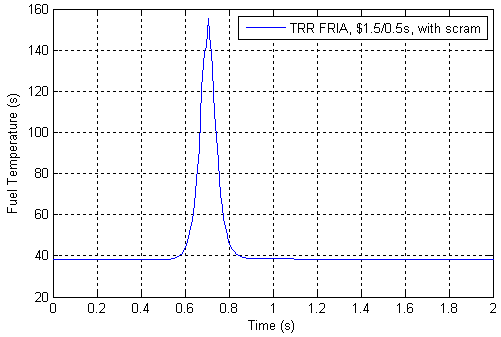

Fig. 10: Changes in fuel temperature as a function of time in FRIA

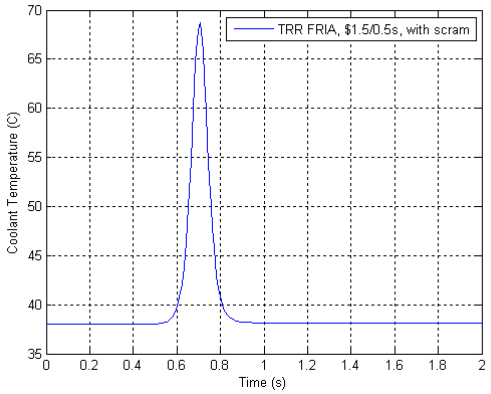

Fig. 11: Changes in coolant temperature as a function of time in FRIA

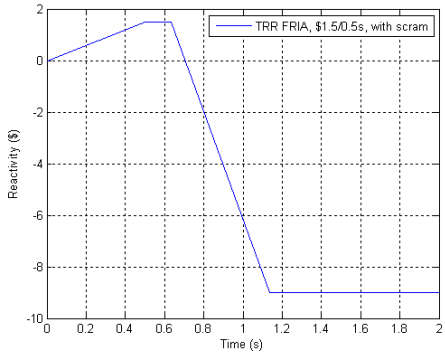

Fig. 12: Changes in reactivity as a function of time in FRIA

5. Conclusion

In modeling reactor dynamics in common codes, fuel burn up and variable fuel and coolant temperature reactivity coefficients are not taken into account (or accounted for with look – up tables),

In modeling reactor dynamics in some common codes, fuel burn up and variable coolant temperature reactivity coefficients are not taken into account (or accounted for with look - up tables), where the burn up is important for large time in reactor analysis, and the coolant temperature is important in transient an safety analysis, so the time of accident cannot be taken into account in a complete manner which can underestimate the situation. In the model presented in this study not only reactor kinetics, reactivity feedbacks due to coolant and fuel temperatures (Doppler effects), xenon, samarium, boron concentration and WIMS and CITVAP codes coupling to extract neutron cross sections and calculate the initial neuron flux are accounted for but also both time dependent delayed neutron fraction and variable temperature feedbacks are taken into account and results are very similar to experimental data. Indeed, the main drawbacks of long running thermal – hydraulic codes that are the amount of time required for preparing the input, pre-processing of the data, huge computational burden and lack of fuel burn up consideration on-line and simultaneously are tackled in this work. Although the model cannot simulate all the thermal hydraulic behaviors of plant it is capable to give us good estimates in short time running and also it models a full fuel cycle in a nuclear reactor, with simulating the short timescale kinetic behavior of the reactor as well as the long time-scale dynamics that occur with fuel burn up. When the equations are solved simultaneously with a nonlinear equation solver, the end result is a code with the unique capability of modeling transients at any time during a fuel cycle.

Although this model is derived and verified with a research reactor, but it's also applicable to power reactors and only modification is needed for input card in WIMS and CITVAP codes.

ACKNOWLEDGEMENT

Here, I admit the supports of Islamic Azad University of Shiraz in the process of working on this research.

References

Arab-Alibeik H and Setayeshi (2003). An adaptive-cost-function optimal controller design for a PWR nuclear reactor. Annals of Nuclear Energy, 30: 739-754.

Arab-Alibeik H and Setayeshi S (2003). Improved temperature control of a PWR nuclear reactor using an LQG/LTR based controller. IEEE Transactions on Nuclear Science, 50: 211-218.

Arab-Alibeik H and Setayeshi S (2005). Adaptive control of a PWR core power using neural networks. Annals of Nuclear Energy, 32: 588–605.

Bank RE, Coughran WM, Fichtner W, Grosse EH, Rose DJ and Smith RK (1985). Transient simulation of silicon devices and circuits. IEEE Transactions on Computer-Aided Design of Integrated Circuits and Systems, 4(4): 436-451.

Barati R, Setayeshi S (2012). Human Reliability Analysis of the Tehran Research Reactor using SPAR - H Method. Nuclear Technology and Radiation Protection, 27: 319-332.

Barati R, Setayeshi S (2013). Functional reliability evaluation of an MTR-pool type research reactor core using the load–capacity interference model. Annals of Nuclear Energy, 58: 151-160.

Bell GI and Glasstone S (1970). Nuclear Reactor Theory. Van Nostrand Reinhold, New York.

Ben-Abdennour A, Edwards RM, Lee KY (1992). LQG/LTR robust control of nuclear reactors with improved temperature performance. IEEE Transactions on Nuclear Science, 39: 2286-2294.

Benedict M, Pigford TH, Levi HW (1981). Nuclear Chemical Engineering. McGraw-Hill, Berlin.

Bogacki P, Shampine LF (1989). A 3(2) pair of Runge-Kutta formulas. Applied Mathematics Letters, 2(4): 321-325.

Bousbia Salah A, Hamidouche T (2005). Analysis of the IAEA research reactor benchmark problem by the RETRAC-PC code. Nuclear Engineering and Design, 235: 661-674.

Dormand JR and Prince PJ (1980). A family of embedded Runge-Kutta formulae. Journal of Computational and Applied Mathematics, 6(1): 19-26.

Duderstadt J and Hamilton L (1976). Nuclear Reactor Analysis. John Wiley & Sons, New York.

Edwards, R.M., Lee, K.Y., Ray, A., 1992. Robust optimal control of nuclear reactors and power plants. Nuclear Technology, 98(2): 137-148.

El-Messiry AM (2000). Reactivity accidents analysis during natural core cooling operation of ETRR-2 Annals of Nuclear Energy, 27: 1427-1439.

Espinosa-Paredes G and Espinosa-Martínez EG (2009). Fuel road model based on Non-Fourier heat conduction equation. Annals of Nuclear Energy, 36: 680-693.

Espinosa-Paredes G and Nuñez-Carrera A (2008). SBWR Model for Steady State and Transient Analysis. Science and Technology of Nuclear Installations, Article ID 428168, 18.

Espinosa-Paredes G and Y Álvarez-Ramírez J (2003). Scope and limitations of the structural and dynamic analysis of a thermal-hydraulic model. Annals of Nuclear Energy, 30(8): 931-942.

Espinosa-Paredes G, Álvarez-Ramírez J, Núñez-Carrera A, García-Gutiérrez A, Martínez-Méndez J (2004). Dynamic comparison of three and four-equation reactor core models in a full-scope power plant training simulator. Nuclear Technology, 145(2): 150-162.

Espinosa-Paredes G, Polo-Labarrios, MA, Vázquez-Rodríguez A (2012). Sensitivity and uncertainty analysis of the time-fractional telegrapher´s equation for neutron motion. Progress in Nuclear Energy, 61: 69-77.

Forsythe G, Malcolm M, Moler C (1977). Computer Methods for Mathematical Computations. Prentice-Hall, New Jersey.

Gaheen MA, Sayed E, Naguib AM, Nagy MS (2007). Simulation and analysis of IAEA benchmark transients. Progress in Nuclear Energy: 217-229.

Gear CW (1971). Numerical Initial Value Problems in Ordinary Differential Equation. Prentice-Hall, Englewood Cliffs, NJ.

Hainoun A (2003). Thermalhydraulic Design And Safety Analysis Of Research Reactors. IAEA-CN-100/137, International Conference on Research Reactor Utilization, Safety, Decommissioning, Fuel and Waste Management, Santiago, Chile.

Hamidouche T, Bousbia-Salah A, Adorni M, D'Auria F (2004). Dynamic calculations of the IAEA safety MTR research reactor benchmark problem using RELAP5/3.2 code. Annals of Nuclear Energy 31: 1385-1402.

Housiadas C (2002). Lumped parameters analysis of coupled kinetics and thermal-hydraulics for small reactors. Annals of Nuclear Energy, 29: 1315-1325.

Johnson M, Lucas S and Tsvetkov P (2010). Modeling of Reactor Kinetics and Dynamics. Laboratory IN, Idaho Falls, ID, 83415.

Kahaner DC and Moler Nash S (1989). Numerical Methods and Software. Prentice-Hall, New Jersey.

Kazeminejad H (2006). Reactivity insertion limits in a typical pool-type research reactor cooled by natural circulation. Annals of Nuclear Energy, 33: 252-261.

Kazeminejad H (2008). Thermal–hydraulic modeling of flow inversion in a research reactor. Annals of Nuclear Energy, 35: 1813-1819.

Khater H, Abu-EL-Maty T and El-Morshdy SED (2007). Thermal-hydraulic modeling of reactivity accident in MTR reactors. Annals of Nuclear Energy, 34(9): 732-742

Klopfenstein RW (1971). Numerical differentiation formulas for stiff systems of ordinary differential equations. RCA Review, 32: 447-462.

Lu Q, Qiu S and Su GH (2009). Development of a thermal–hydraulic analysis code for research reactors with plate fuels. Annals of Nuclear Energy, 36: 433–447.

March- Leuba J (1986). A reduced-order model of boiling water reactor linear dynamics. Nuclear Technology, 75(1): 15-22.

Mariy AH, EL-Morshdy SE, Khater HA, Abdel-Raouf AA (2003). Transient thermal–hydraulic modeling of ETRR-2 for off-site power loss Proceedings of an International Conference, 10-14 November. IAEA-CN-100/ 64, Research Reactor Utilization, Safety, Decommissioning, Fuel and Waste Management, Santiago, Chile.

Nabbi R (1995). Numerical fluid flow and heat transfer calculation (HEATHYD code). IAEA-

TECDOC 1004, In the Final Research Co-ordination Meeting Held in Dalat Vietnam, 27-48.

Nuñez-Carrera A, Espinosa-Paredes G, Francois JL (2004). Model for transient and stability análisis of a BWR core with thorium-uranium fuel. In the Transactions of 2004 Annual Meeting, ANS, 90: 563-565.

Rubio RO (1993). Borges. MTR_PC, Nuclear Engineering Division, INVAP, Argentina.

Sadighi M, Setayeshi S, Salehi AA (2002). Neutron Flux Flattening in PWRs Using Neural Networks in Fuel Management. IEEE Transactions on Nuclear Science, 49(3): 1574-1578.

SARforTRR (2002). Safety analysis report for Tehran research reactor. Nuclear Research Center of the Atomic Energy Organization of Iran, Tehran.

Shampine LF (1994). Numerical Solution of Ordinary Differential Equations. Chapman & Hall, New York.

Shampine LF and Gordon MK (1975). Computer Solution of Ordinary Differential Equations: the Initial Value Problem. W. H. Freeman, SanFrancisco.

Shampine LF and Hosea ME (1996). Analysis and Implementation of TR-BDF2. Applied Numerical Mathematics, 20(1): 21-37.

Shampine LF and Reichelt MW (1997). The MATLAB ODE Suite. SIAM Journal on Scientific Computing, 18: 1-22.

Shampine LF, Reichelt MW and Kierzenka JA (1999). Solving Index-1 DAEs in MATLAB and Simulink. SIAM Review, 41: 538-552.

Stacey W (2007). Nuclear Reactor Physics. 2nd Edition, WILEY-VCH Verlag GmbH & Co. KGaA, Weinheim.

Tashakor S, Jahanfarnia G and Hashemi-Tilehnoee M (2010). Numerical solution of the point kinetics equations with fuel burn-up and temperature feedback. Annals of Nuclear Energy, 37(2): 265–269.

Villarino E and Carlos L (1993). CITVAP v3.1 Reactor calculation code. MTR_PC, Nuclear Engineering Division. INVAP, Argentina.

Wang Q, Zhang D, Chen W, Chen Z (2011). Real-time simulation of response to load variation for a ship reactor based on point-reactor double regions and lumped parameter model. Annals of Nuclear Energy, 38: 1156–1160.

Woodruff WL (1984). A kinetics and thermal–hydraulic capability for the analysis of research reactors. Nuclear Technology, 64: 196-206.

Woodruff WL, Hanan NA, Smith RS, Matos JE (1996). A comparison of the PARET/ANL and RELAP5/Mod3 codes for the analysis of IAEA benchmark transients. In the International Meeting on Reduced Enrichment for Research and Test Reactors, Seoul, South Korea.